http://dx.doi.org/10.5012/bkcs.2013.34.2.609

Influence of Different A Elements on Bonding and Elastic Properties of Zr_2AC (A = Al, Si, P, S): A Theoretical Investigation

Dae-Bok Kang

Department of Chemistry, Kyungsung University, Busan 608-736, Korea. E-mail: dbkang@ks.ac.kr
Received October 24, 2012, Accepted December 5, 2012

Extended Hückel tight-binding band structure calculations are used to address the chemical bonding and elastic properties of Zr_2AC (A=Al, Si, P, and S). Elastic properties are interpreted by analyzing the density of states and the crystal orbital overlap population for the respective phases. Our results show that the bulk modulus of these ternary compounds is determined by the strength of Zr-A bonds.

Key Words : Electronic structure, Elastic properties, MAX phase

Introduction

Materials, known as "MAX" phases, are very promising candidates for a number of structural applications, owing to their low density, high elastic modulus, excellent damage tolerance and thermal shock resistant properties. The MAX-phase is a designation given to ternary compounds with the composition of $M_{n+1}AX_n$, where n = 1, 2 or 3, M is an early transition metal, A is an A-group (mostly IIIA and IVA) element, and X is C or N. What makes the MAX phases fascinating and potentially useful is a remarkable combination of chemical, electrical, and mechanical properties which in many ways display the characteristics of metals and ceramics. For example, they typically show excellent resistance to oxidation and maintain their specific stiffness and stability even at high temperatures, like ceramics, but at the same time they exhibit good thermal and electrical conductivity and significant plasticity that leads to easy machinability, like metals.[1-8]

The MAX-phase carbides adopt a hexagonal crystal structure consisting of layers of edge-sharing M_6C octahedra interleaved with planar close-packed A-group element layers. The edge-sharing M_6C octahedral building blocks are quite similar to those found in the rock salt structure of the corresponding binary carbides MC that are important high-temperature hard materials with extremely high chemical and thermal stability.[9] It should be pointed out that the mechanical properties of these layered ternaries are very different from those of MC. The mechanical properties such as high-temperature stiffness and damage tolerance mentioned above are rarely exhibited simultaneously by their binaries MC. These unique elastic properties of MAX-phase carbides are attributed to their layered structure and the bonding characteristics of alternately stacking of the strong M-C bonds and relatively weak M-A bonds along the *c* direction.

Over the last few years a concerted effort was devoted to the experimental and theoretical studies[10-26] of these compounds to understand the relationship between their crystal structures and elastic properties. Zhou and co-workers reported that the mechanical properties of M_2AC ceramics are dominated by the weak coupling between M-C octahedron slabs and weakly bonded A layers.[24-26] They suggested that by properly tuning the valence electron concentration an enhancement in mechanical properties could be achieved. It is reasonable that the strengthening of the softer M-A bonds results in an increase of the bulk modulus. In order to better understand the mechanism of the change of bulk modulus, a thorough theoretical investigation of the bonding properties of the layered ternary carbides is necessary. Bulk modulus measures the resistance of a material to a volume change and fracture, and so the changes in bulk modulus are directly correlated to the interatomic bond strength between adjacent atomic planes within these ternary carbides. The high modulus can be traced to the strong covalent bonds, while the relatively weak M-A bonding is believed to be responsible for easy basal slip and low shear strength.

In the present paper we therefore concentrate on exploring the relations between the elastic properties and the electronic structure of Zr_2AC (A=Al, Si, P, and S) as a function of the filling of p states of A elements. Special attention is devoted to the bonding properties of Zr-A bonds. The knowledge of the bonding features of the Zr_2AC compounds with different A-site elements will provide a guide for improving mechanical properties of the MAX phases. We use the total and projected density of states (PDOS) and crystal orbital overlap population (COOP) techniques to examine the chemical bonding features in Zr_2AC phases. The COOP curves are indicative of the nature and strength of the bonds between constituent atoms, with positive and negative regions indicating bonding and antibonding states, respectively. These calculations have been performed using the extended Hückel tight-binding (EHTB) method[27,28]; parameters are given in Table 1. In this work all calculations were carried out at the theoretical lattice constants obtained from ref. 29.

Structure Description

The crystal structure of Zr_2AC can be described as the

Table 1. Parameters for EH calculations

Atom	Orbital	H_{ii}, eV	ζ_1	ζ_2	c_1	c_2
Zr	4d	-10.2	3.835	1.505	0.6210	0.5769
	5s	-8.0	1.817			
	5p	-5.4	1.776			
C	2s	-21.4	1.625			
	2p	-11.4	1.625			
Al	3s	-12.3	1.167			
	3p	-6.5	1.167			
Si	3s	-17.3	1.383			
	3p	-9.2	1.383			
P	3s	-18.6	1.75			
	3p	-14.0	1.30			
S	3s	-20.0	2.122			
	3p	-13.3	1.827			

hexagonal closest packing of Zr and A atoms with alternating blocks of zirconium carbide (Zr_2C) and networks of A atoms. The Zr_2C blocks contain a single layer of edge-sharing Zr_6C octahedra adjacent to the networks of A atoms, and the Zr_2AC structure possesses a layer stacking sequence (along the *c*-axis) of C-Zr-A-Zr-C-Zr-A-Zr-C as shown in Figure 1. The Zr layer exists in every other layer and the C atoms occupy octahedral holes or anti-prismatic sites between slabs of edge-sharing Zr_6A trigonal prisms. It crystallizes in the hexagonal $P6_3/mmc$ space group (no. 194) with two formula units per unit cell. The layered structure consists of three types of slabs, lower Zr-A-Zr, middle Zr-C-Zr, and upper Zr-A-Zr along the *c*-axis (Figure 1). Both Zr-A-Zr slabs are made of edge-sharing Zr_6A trigonal prisms. The hexagonal lateral Wyckoff positions of Zr and A atoms in the lower Zr-A-Zr slab are the 4*f* site (1/3, 2/3) and the 2*d* site (2/3, 1/3), respectively. Those in the upper Zr-A-Zr slab exchange their sites relative to the lower Zr-A-Zr slab. The C atoms in the middle Zr-C-Zr slab occupy only the 2*a* site (0, 0). No Zr and A atoms exist right below and above the C atoms along the *c*-axis. The structure is thus defined by two lattice constants *a* and *c* and the only free positional parameter *z* for the Zr atoms. Table 2 shows a summary of the structural data for Zr_2AC (A=Al, Si, P, S).[29]

The bulk modulus values of elasticity are also listed in Table 2. One notices that the bulk modulus of Zr_2PC is higher than the other Zr_2AC compounds. The bulk modulus increases as the A-group element moves from Al to P across the periodic table. This extensive increase in bulk moduli can be understood by considering the changes in the electronic structure and Zr-A bond strength associated with the filling of A 3p states driven to deeper energy in Zr_2AC. Detailed electronic and bonding properties are analyzed in the next section.

Results and Analysis

Density of States. In order to elucidate the nature of the electronic band structure of Zr_2AC (A=Al, Si, P, S), we have calculated the PDOS for these compounds. The total and

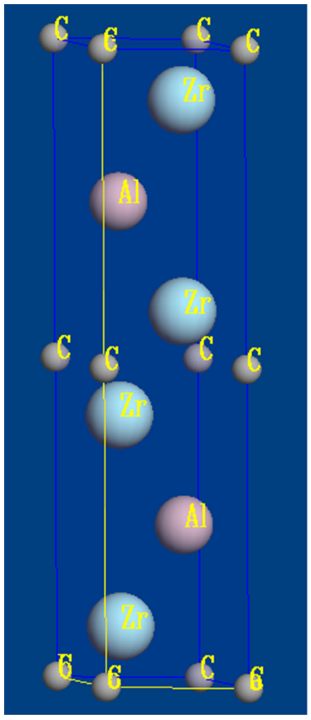

Figure 1. Primitive unit cell of Zr_2AlC.

Table 2. Structural data and bulk moduli (B) for Zr_2AC (A=Al, Si, P, S)

Compound	*a* (Å)	*c* (Å)	z	B (GPa)
Zr_2AlC	3.308	14.680	0.08436	150
Zr_2SiC	3.338	13.834	0.09215	173
Zr_2PC	3.433	12.173	0.10280	186
Zr_2SC	3.485	12.524	0.09741	163

projected DOS curves are displayed in Figure 2. In all carbides, the Fermi level (E_F) crosses the lower part of the Zr 4d states. DOS distributions demonstrate strong mixing effects for Zr 4d, A 3p, and C 2p states leading to the formation of covalent Zr-C and Zr-A bonds. As for the great majority of the MAX phases, there is no band gap and the DOS has a finite value at E_F. This finding confirms the metallic properties of these materials. We can see from the DOS that the Zr d states are mainly contributing to the DOS at E_F and should play a dominant role in electrical transport. Carbon does not contribute significantly to the DOS at E_F and therefore is not involved in the conduction properties. We can say the same about the A atoms.

As seen in Figure 2(a), the valence bands of Zr_2AlC form three main groups. The lowest energy bands localized at around −23 eV originate from 2s orbital of carbon with a minor admixture of Zr 4d orbitals. These bands are separated from the upper occupied bands. The upper valence bands, ranging approximately from −14.5 to −12.5 eV, are mainly composed of C 2p orbitals which overlap with the Zr 4d orbitals considerably. This is an indication of the strong mixing of their states. An obvious reason that the C 2p orbitals interact better with the Zr 4d orbitals is a good

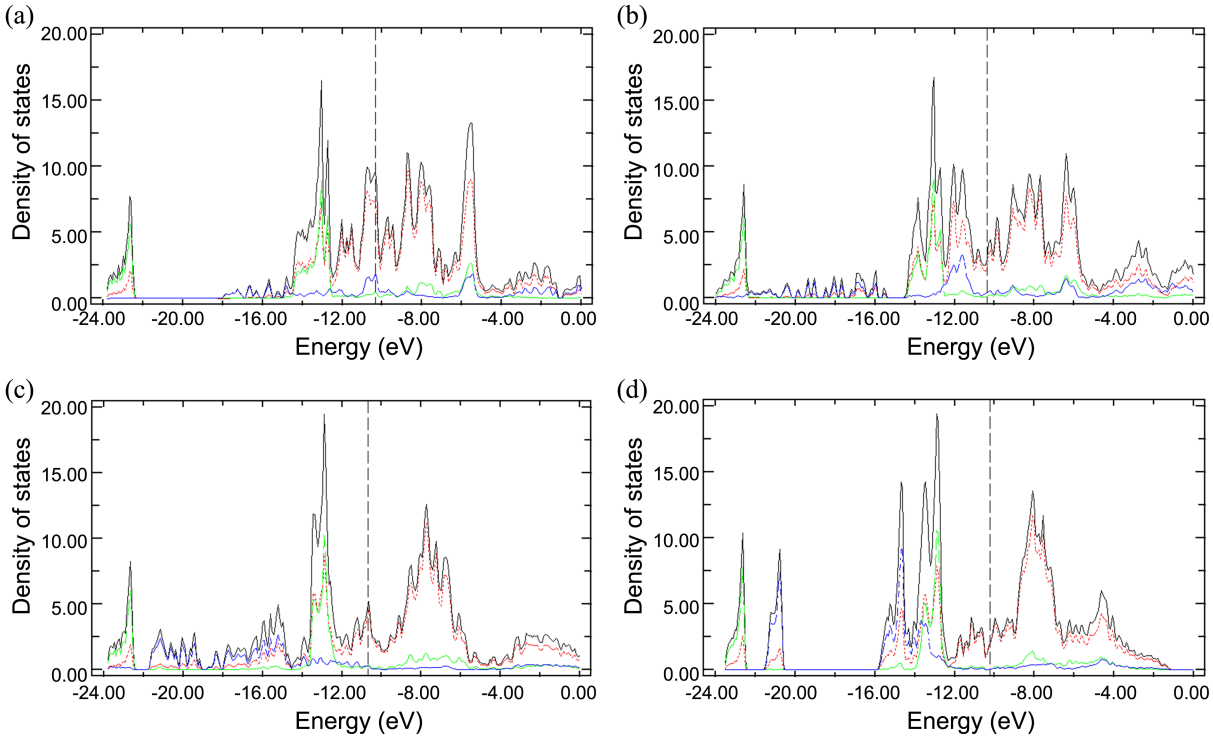

Figure 2. Total DOS (black line) and the contributions of Zr (red line), C (green line), and A (blue line) orbitals to it in (a) Zr_2AlC, (b) Zr_2SiC, (c) Zr_2PC, and (d) Zr_2SC. The vertical dashed lines denote the Fermi level.

energy match between them. It is this strong covalent interaction between C 2p and Zr 4d orbitals that explains the structure stability of Zr_2AlC, a general trend in MAX phases. The structure ranging from −12.5 eV to −5 eV arises mainly from Zr 4d orbitals. The energy location and width of C 2s, C 2p, and Zr 4d bands are close to those for ZrC. The DOS in the vicinity of the Fermi level is derived from Zr 4d states with an admixture of Al 3p states. The higher lying structure up to −5 eV consists of a mixture of Zr d and C/Al p states. Their antibonding states are seen above E_F in the energy range −9 to −5 eV. Also, the PDOS profile exhibits another interesting feature: the intense bonding peaks of C 2p-Zr 4d orbitals (−14.5 to −12.5 eV) are much more delocalized than those of Zr 4d-Al 3p orbitals (−11 to −10 eV) due to the overlap of better energy match between the interacting orbitals of the constituent atoms. This may result in a stronger Zr-C covalent bonding. This conclusion is consistent with the fact that in the majority of MAX phases, the M-X bonds are stronger than the M-A bonds.

In the Zr_2AC structure, the Zr_6C octahedra are compressed along *z* in all compounds. The in-plane Zr-Zr distance in Zr_2AlC is 3.31 Å, while the interlayer Zr-Zr distance is 3.13 Å. For comparison, the Zr-Zr distance in bulk Zr metal is 3.17 Å. Thus, d-d interactions between the Zr atoms in the Zr_2C sublattice should play an appreciable role in the bonding. The Zr-C distance is 2.28 Å, which is slightly less than that in binary carbide ZrC (2.35 Å).[30] The Zr-C bonds in the ternaries are slightly shorter on average than the corresponding Zr-C bonds in the binaries, and thus presumably strong orbital interactions of Zr with C should also be expected. Therefore, the strong Zr-C bonds are well preserved in the ternary carbides. The Zr-Al distance is 3.09 Å. This distance is a lot larger than the sum of single-bond metallic radii for Zr and Al (2.70 Å).[31] This probably indicates the weaker interaction between Zr and Al in contrast to the Zr-C interaction. The Al-Al bond distance in Zr_2AlC (3.31 Å) is much longer than the one in pure Al (2.86 Å). The bonding contribution of the Al atoms results from their bonding to the Zr_6C blocks *via* presumably p-d overlap out of the basal planes, and not from bonding formed between them. This overlap is stronger in Zr_2SiC than in Zr_2AlC, which will be discussed shortly.

The DOS for Zr_2SiC is illustrated in Figure 2(b). The basic feature of the band structures of Zr_2SiC and Zr_2AlC is similar. However, Zr 4d-Si 3p bonding states, ranging from −12.5 to −11 eV in Figure 2(b), are shifted to lower energy compared to Zr 4d-Al 3p bonding states at −11 to −10 eV in Figure 2(a). This result indicates stronger bond strength of Zr-Si in Zr_2SiC than Zr-Al in Zr_2AlC and thereby Zr_2SiC displays higher elastic bulk modulus than Zr_2AlC. Another common feature is the presence of the metallic bonding states near the Fermi level that originate from the d-d interactions between the Zr atoms in Zr-C-Zr slab. They contribute slightly to the bonding.

As A-group element changes from Si to P, Zr_2PC exhibits totally different bonding characteristics from Zr_2SiC. It is interesting to note from Figure 2(c) that the P 3p-Zr 4d bonding states are found at the lower energy range (−18 to −14 eV) than the C 2p-Zr 4d bonding states at around −13.5 to −12.5 eV. The orbital interactions between P 3p and Zr 4d

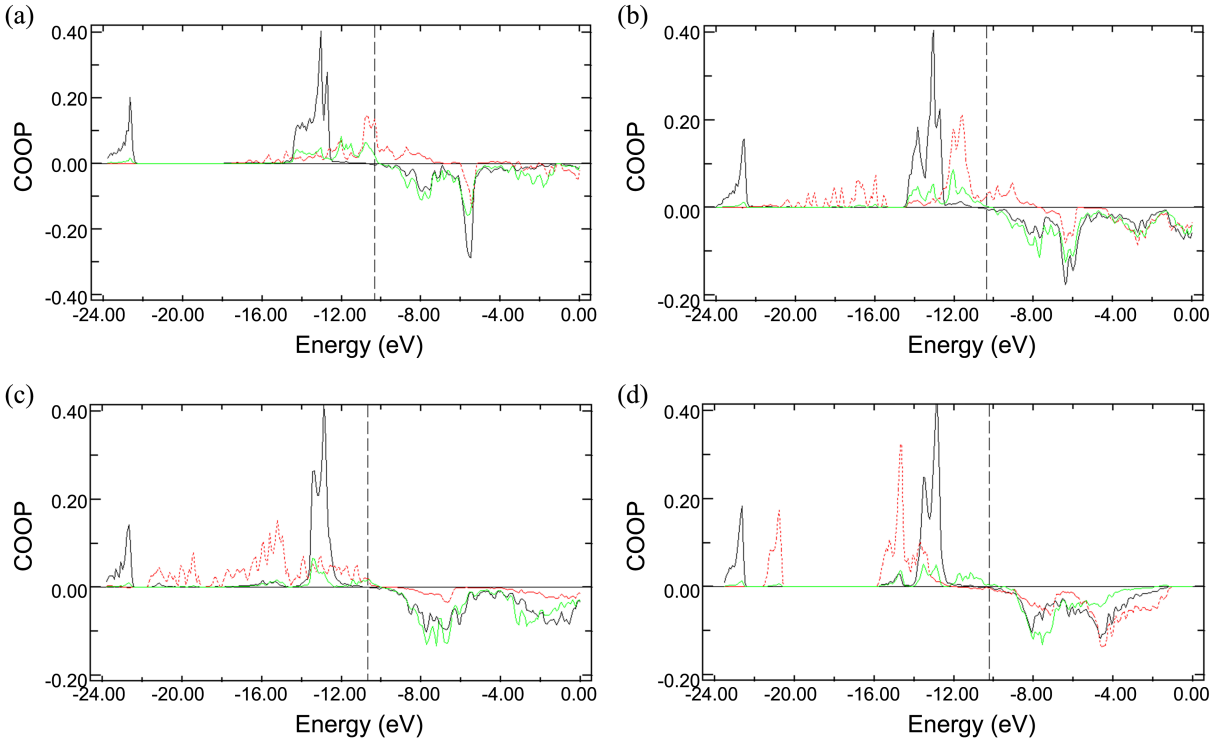

Figure 3. Crystal orbital overlap populations for the Zr-C (black line), Zr-A (red line), and Zr-Zr (green line) bonds in (a) Zr_2AlC, (b) Zr_2SiC, (c) Zr_2PC, and (d) Zr_2SC. The vertical dashed lines denote the Fermi level.

give rise to a fairly dispersed DOS. This suggests that Zr-P bond strength is greater than Zr-C bond. Such a strong M-A bond is unusual in MAX phases. This is expected to contribute considerably to the phase stability of Zr_2PC and affects its structural and mechanical properties. The Zr-P separation is 2.67 Å, which is slightly larger than a value of 2.55 Å expected for a Zr-P single bond.[31] Consequently, these two orbitals should have a very large overlap. It is worth noting that this interaction is sizable in spite of a large energy difference between the two orbitals involved. The strengthened Zr-P bonding increases the overall strength of this compound and the exceptionally high bulk modulus of Zr_2PC is attributed to contribution from the strong Zr-P bonds.

For Zr_2SC, it exhibits slightly different electronic structure from Zr_2PC. As displayed in Figure 2(d), the PDOS of S 3p orbitals, extending from approximately −16 to −14 eV, is narrow and is mainly derived from less mixing with Zr 4d orbitals because the Zr and S atoms are 2.78 Å apart. Although the covalent radius of S atom is smaller than that of P, the bond distance of Zr-S is larger than that of Zr-P. The longer bond distance between Zr and S indicates that the bond strength between them is weakened compared to the Zr-P bond, and hence the weakened Zr-S bond strength gives rise to negative contribution to the elasticity of Zr_2SC.

At this point the discussion of the mixing features solely from the PDOS cannot give detailed information about the chemical bonding in these compounds. A further step must be undertaken by examining the COOP. Let us now turn our attention to their bonding properties.

Crystal Orbital Overlap Population. The properties of covalent bonding can be assessed further by Mulliken population analysis. This analysis provides more quantitative information about the chemical bonding by the use of COOP. We show in Figure 3 the calculated COOP curves for atom pairwise interactions in the four Zr_2AC (A=Al, Si, P, S) systems. Note the general characteristics of COOP curve: positive regions that are bonding and negative regions that are antibonding.

Analysis of the orbital interactions *via* COOP indicates that both the Zr-C bonding and Zr-Zr bonding are optimized in all compounds. From Figures 3(a) and 3(b), it is seen that the bonding states of Zr 4d-Al 3p and Zr 4d-Si 3p are present at approximately −11 and −12 eV, respectively, and stronger Zr 4d-C 2p bonding states are lying deeper in energy (−14.5 to −12.5 eV). Not all bonding states are filled for both Zr-Al and Zr-Si interactions. In fact, the degree of their bond strength does not only depend on the relative COOP peak positions below the Fermi level but also on the relative intensity of the peaks. For a given bond, the integrated overlap population up to the Fermi level reflects its bond strength. The difference in the bond strength of Zr-Al and Zr-Si is attributed to the change of the electronic structure with increasing the filling of A 3p states from Al to Si. As shown in Figures 3(a) and 3(b), the peak of Zr 4d-Si 3p bonding states slightly shifts to lower energy and becomes intense, compared with that of Zr 4d-Al 3p bonding states. In Zr_2AlC and Zr_2SiC, below E_F, the Zr-C bonding interactions predominate. All antibonding counterparts of Zr-Al/Si as well as Zr-C interactions can be seen in the conduction

Table 3. Overlap populations (OP) for Zr-C, Zr-A, Zr-Zr, and A-A bonds in Zr_2AC (A=Al, Si, P, S) and ZrC

Compound	Bond	Bond length (Å)	OP
Zr_2AlC	Zr-C	2.276	0.41
	Zr-Al	3.092	0.19
	Zr-Zr	3.128, 3.308	0.15
	Al-Al	3.308	0.11
Zr_2SiC	Zr-C	2.311	0.41
	Zr-Si	2.913	0.31
	Zr-Zr	3.196, 3.338	0.13
	Si-Si	3.338	0.09
Zr_2PC	Zr-C	2.344	0.40
	Zr-P	2.672	0.42
	Zr-Zr	3.193, 3.433	0.08
	P-P	3.433	0.04
Zr_2SC	Zr-C	2.353	0.40
	Zr-S	2.775	0.32
	Zr-Zr	3.163, 3.485	0.10
	S-S	3.485	-0.01
ZrC	Zr-C	2.351	0.40
	Zr-Zr	3.325	0.07

bands (approximately −7 to −5 eV). Therefore, the Zr-Si bonding results in the stronger coupling between the transition metal carbide slabs and A-group atom layers, compared to Zr-Al bonding.

The elastic properties in Zr_2AC (A=Al, Si, P, S) compounds are strongly related to the covalent bond strength of Zr-A bonds with the filling of A 3p states driven to deeper energy. More filled bonding states of Zr-Si bonds, compared to Zr-Al bonds, nicely explain the increase of bulk modulus from Zr_2AlC to Zr_2SiC. In the case of the Zr-P interactions, as shown in Figure 3(c), more delocalized bonding states are seen to extend over a wider energy range −18 to −14 eV. Therefore, the elasticity increases due to the strengthening of Zr-P bond. The bulk modulus decreases on going from Zr_2PC to Zr_2SC. This is due to less bonding states between Zr and S below the Fermi level. The COOP curve of Zr-S bond in Zr_2SC is narrow in its bonding region (Figure 3(d)). And its bond strength is much smaller because of the rapid decrease of coupling overlap with distance. As is known, the p orbitals of the A atom are shifted to lower energy as the filling of the p orbitals is increased. This strongly influences the nature of the energy bands and the Zr-A bonding interactions in these compounds.

The covalent strength of a specified bond can be determined by the total overlap population obtained by summing up the area under the COOP curve up to the Fermi level. We list in Table 3 the calculated overlap populations (OP) and bond distances of covalent bonds in Zr_2AC (A=Al, Si, P, S), together with the corresponding values for ZrC for comparison. The overlap population yields *ca*. 0.41 for Zr-C bonds in these compounds, which is quite comparable to the corresponding value, 0.40, in ZrC. This shows that the degree of covalency for Zr-C bonds in Zr_2AC (A=Al, Si, P, S) is very strong. The increase in OP values of Zr-A bonds in these compounds indicates that there occurs a gradual strengthening of Zr-A bonds when A elements change from Al to Si to P. It presents a maximum for Zr_2PC with a value of 0.42, followed by a sharp decrease for Zr_2SC. This ensures that the Zr-P bonds are stronger in Zr_2PC than the other Zr-A bonds in Zr_2AC (A=Al, Si, P, S).

Conclusion

We have performed EHTB band calculations for the layered Zr_2AC (A=Al, Si, P, S) carbides to study the relationship between their electronic structure and elastic properties. Our results show that the bulk modulus increases as A elements change from Al to P across the periodic table for Zr_2AC. This originates from a gradual strengthening of Zr-A bonds. We also find that more Zr 4d-A 3p bonding states are located deeper in energy below the Fermi level as the filling of A 3p states is increased. Since sulfur has the most filled p states of any of the A elements present in these phases, the Zr-S bonds may be as strong as the Zr-P bonds. However, the Zr-S bond in Zr_2SC is weakened compared to the Zr-P bond in Zr_2PC because of decrease of coupling overlap with large separation between Zr and S. This gives rise to negative contribution to the elasticity of Zr_2SC.

Acknowledgments. This work was supported by the Kyungsung University Research Grant in 2012.

References

1. Barsoum, M. W. *Prog. Solid State Chem*. **2000**, *28*, 201.
2. Finkel, P.; Barsoum, M. W.; El-Raghy, T. *J. Appl. Phys*. **2000**, *87*, 1701.
3. Hettinger, J. H.; Lofland, S. E.; Finkel, P.; Meehan, T.; Palma, J.; Harrel, K. *Phys. Rev. B* **2005**, *72*, 115120.
4. Manoun, B.; Zhang, F. X.; Saxena, S. K.; El-Raghy, T.; Barsoum, M. W. *J. Phys. Chem. Solids* **2006**, *67*, 2091.
5. Drulis, M. K.; Drulis, H.; Hackemer, A. E.; Ganguly, A.; El-Raghy, T.; Barsoum, M. W. *J. Alloys. Compd*. **2007**, *433*, 59.
6. Hu, C. F.; Zhang, J.; Wang, J.; Li, F. G.; Wang, J. Y.; Zhou, Y. C. *J. Am. Ceram. Soc*. **2008**, *91*, 636.
7. Kumar, R. S.; Rekhi, S.; Cornelius, A. L.; Barsoum, M. W. *Appl. Phys. Lett*. **2005**, *86*, 111904.
8. Barsoum, M. W.; El-Raghy, T. *Am. Sci.* **2001**, *89*, 334.
9. (a) Freer, R., Ed. *The Physics and Chemistry of Carbides, Nitrides and Borides*; Kluwer Academic Publishers: Dordrecht, 1990. (b) Ettmayer, P.; Lengauer, W. In *Encyclopedia of Inorganic Chemistry*; J. Wiley: Chichester, 1996; p 519. (c) Toth, L. E. *Transition Metal Carbides and Nitrides*; Academic Press: New York, 1971. (d) Nowotny, H. *Angew. Chem.* **1972**, *84*, 973; *Angew. Chem., Int.Ed. Engl.* **1972**, *11*, 906.
10. Liao, T.; Wang, J. Y.; Zhou, Y. C. *J. Phys. Condens. Matter* **2006**, *18*, L527.
11. Medkour, Y.; Bouhemadou, A.; Roumili, A. *Solid State Commun*. **2008**, *148*, 459.
12. Shein, I. R.; Ivanovskii, A. L. *Phys. C* **2010**, *470*, 533.
13. Romero, M.; Escamilla, R. *Comput. Mater. Sci*. **2012**, *55*, 142.
14. Ghebouli, M. A.; Ghebouli, B.; Fatmi, M.; Bouhemadou, A. *Intermetallics* **2011**, *19*, 1936.
15. Sun, Z. M.; Li, S.; Ahuja, R.; Schneider, J. M. *Solid State Commun*. **2004**, *129*, 589.

16. Bouhemadou, A. *Mod. Phys. Lett. B* **2008**, *22*, 2063.
17. Cover, M. F.; Warschkow, O.; Bilek, M. M. M.; McKenzie, D. R. *J. Phys. Condens. Matter* **2009**, *21*, 305403.
18. Wang, J. M.; Wang, J. Y.; Zhou, Y. C.; Hu, C. F. *Acta Mater.* **2008**, *56*, 1511.
19. Bai, Y. L.; He, X. D.; Li, Y. B.; Zhu, C. C.; Li, M. W. *Solid State Commun.* **2009**, *149*, 2156.
20. Zhou, Y. C.; Sun, Z. M.; Wang, X. H.; Chen, S. Q. *J. Phys. Condens. Matter* **2001**, *13*, 10001.
21. Sun, Z. M.; Ahuja, R.; Li, S.; Schneider, J. M. *Appl. Phys. Lett.* **2003**, *83*, 899.
22. Sun, Z. M.; Music, D.; Ahuja, R.; Li, S.; Schneider, J. M. *Phys. Rev. B* **2004**, *70*, 092102.
23. Hug, G. *Phys. Rev. B* **2006**, *74*, 184113.
24. Wang, J. Y.; Zhou, Y. C. *Phys. Rev. B* **2004**, *69*, 214111.
25. Liao, T.; Wang, J. Y.; Zhou, Y. C. *J. Mater. Res.* **2009**, *24*, 556.
26. Liao, T.; Wang, J. Y.; Zhou, Y. C. *Phys. Rev. B* **2006**, *73*, 214109.
27. Whangbo, M.-H.; Hoffmann, R. *J. Am. Chem. Soc.* **1978**, *100*, 6093.
28. Whangbo, M.-H.; Hoffmann, R.; Woodward, R. B. *Proc. R. Soc. A* **1979**, *366*, 23.
29. Kanoun, M. B.; Goumri-Said, S.; Reshak, A. H.; Merad, A. E. *Solid State Sci.* **2010**, *12*, 887.
30. Vojvodic, A.; Ruberto, C. *J. Phys. Condens. Matter* **2010**, *22*, 375501.
31. Pauling, L. *The Nature of the Chemical Bond*; Cornell University Press: Ithaca, New York, 1960.